Volume 1 | Number 1 | Jan 2013 | Pages 1–100

PCCP

Physical Chemistry Chemical Physics
www.rsc.org/pccp

ROYAL SOCIETY OF CHEMISTRY

ROYAL SOCIETY OF CHEMISTRY

www.rsc.org/pccp

Role of Electron Spin Dynamics on Solid-State Dynamic Nuclear Polarization Performance

Ting Ann Siaw,[a] Matthias Fehr,[b] Alicia Lund,[b] Allegra Latimer,[b] Shamon A. Walker,[a] Devin T. Edwards,[c] and Song-I Han[a,b]*

[a] *Department of Chemical Engineering, University of California Santa Barbara, Santa Barbara, CA 93106, USA.*
[b] *Department of Chemistry and Biochemistry, University of California Santa Barbara, Santa Barbara, CA 93106, USA.*
[c] *Department of Physics, University of California Santa Barbara, Santa Barbara, CA 93106, USA.*
* Corresponding author. Address: Department of Chemistry and Biochemistry, University of California Santa Barbara, Santa Barbara, CA 93106, USA. Tel: +1 (805) 893 4858, Fax: +1 (805) 893 4120, e-mail: songi@chem.ucsb.edu

Abstract

For the broadest dissemination of solid-state dynamic nuclear polarization (ssDNP) enhanced NMR as a materials characterization tool, the ability to employ generic mono-nitroxide radicals as spin probes is critical. A better understanding of the factors contributing to ssDNP efficiency is needed to rationally optimize the experimental condition for the practically accessible spin probes at hand. This study seeks to advance the mechanistic understanding of ssDNP by examining the effect of electron spin dynamics on the ssDNP performance at liquid helium temperatures (4-40 K). The key observation is that bi-radicals and mono-radicals can generate comparable nuclear spin polarization at 4 K and 7 T, which is in contrast to ssDNP at liquid nitrogen temperatures (80-150 K) that find bi-radicals to clearly outperform mono-radicals. To rationalize this observation, we analyze the change in the DNP-induced nuclear spin polarization (P_n) and the characteristic ssDNP signal buildup time as a function of electron spin relaxation rates that are modulated by the mono- and bi-radical spin concentration. Changes in P_n are consistent with a systematic variation in the product of the electron spin-lattice relaxation time and the electron spin flip-flop rate that constitutes an integral saturation factor of an inhomogeneously broadened EPR spectrum. We show that the comparable P_n achieved with both radical species can be reconciled with a comparable integral EPR saturation factor. Surprisingly, the largest P_n is observed at an intermediate spin concentration for both the mono- and bi-radicals. At the highest radical concentration, the stronger inter-electron spin dipolar coupling favors ssDNP, while oversaturation diminishes P_n, as experimentally verified with the observation of a maximum P_n at an intermediate, not the maximum, microwave (µw) power. At the maximum µw power, oversaturation reduces the electron spin population differential that must be upheld between electron spins that span a frequency difference matching the ^{1}H NMR frequency—characteristic of the cross effect DNP. This new mechanistic insight allows us to rationalize experimental conditions where generic mono-nitroxide probes can offer competitive ssDNP performance to that of custom designer bi-radicals, and thus helps vastly expand the application scope of ssDNP for the study of functional materials and solids.

1. Introduction

The development of solid state DNP (ssDNP) instrumentation, methods and theory has peaked in recent years, and promise to transform NMR-based characterization of solids as we know it, by

enabling the detection of dilute species, material surfaces and biological systems otherwise inaccessible[1–9]. Still, higher, more reliable and rationally predictable performance is needed to establish ssDNP-enhanced nuclear magnetic resonance (NMR) as a broadly applicable characterization tool for a broad range of samples and solvent systems. Optimal operating conditions for ssDNP have been explored for various experimental settings (temperature, magnetic field, polarizing agent, solvent, nuclei, µw power, etc.)[10–13], but cannot be reliably predicted for different sample systems, given the lack of a generally agreed upon mechanistic understanding of ssDNP and the many factors contributing to its performance. Thus, optimal ssDNP operating conditions for a given sample is largely empirically determined. In recent studies, rigid bi-nitroxide radicals such as 1-(TEMPO-4-oxy)-3-(TEMPO-4-amino)propan-2-ol (TOTAPOL)[14,15] and variants of bis-TEMPO-bisketal (bTbk)[16] or a tri-nitroxide radical variant, 4-[N,N-di(2-hydroxy-3-(TEMPO-4'-oxy)-propyl)]-amino-TEMPO (DOTOPA-TEMPO)[11] have been presented as superior polarizing agents for ssDNP, clearly outperforming mono-TEMPO radicals at ~100 Kelvin (K) and high magnetic fields at or above 9 Tesla (T), by a factor of five and higher, comparatively[15,16]. These bi-radicals or tri-radicals are designed to have a fixed or much narrower distribution of electron-electron distances and orientations to more efficiently select for the cross effect (CE) mechanism, which relies on a concerted electron-electron-nuclear three-spin flip process[17]. The frequency difference between two electron spins undergoing dipolar coupling-mediated flip-flops has to match the nuclear Larmor frequency at the operating magnetic field, in order to drive the transfer of spin polarization from electron to nuclear spins. It has been observed that the inter-electron spin distance and relative molecular orientation of the bi-radicals[15] can tune the ssDNP performance—defined here as the amount of nuclear spin polarization generated via DNP. Meanwhile, high nuclear spin polarization in the tens of percent range[10,11,18,19] has been achieved by DNP using generic mono-nitroxide radicals when operating at below 40 K temperatures, while other recent studies hint at the importance of optimal electron spin relaxation times for generating large nuclear spin polarizations, where either too short or too long electron spin-lattice relaxation times, T_{1e}, may diminish the ssDNP performance[16,20]. These effects have been most clearly demonstrated by studies where T_{1e} is directly and exclusively modulated by the addition of Gadolinium complexes[21–23]. Specifically, a previous study involving the authors here reported on the observation of ^{1}H spin polarization as high as 61 % using 4-Amino-2,2,6,6-tetramethylpiperidin-1-yloxyl (4-AT) at 4 K and 7 T[18], which corresponds to a steady state DNP enhancement factor (ε_{ss}) of 336. This suggests that favorable spin dynamics for ssDNP can enhance the ultimate ssDNP performance of a generic mono-radical probe that is competitive with state-of-the-art designer bi-radicals. Substantiating this hypothesis is the core objective of the study presented here. The inter-related effects of the bi-radical vs. the mono-radical architecture and the nuclear and electron spin relaxation times for optimal DNP performance at different fields, temperatures and radical concentrations are unclear, as direct and concurrent studies of DNP and pulsed electron paramagnetic resonance (EPR) measurements conducted under comparable experimental conditions are rare, which gap this study seeks to fill.

The prospect of exploiting mono-radicals for ssDNP studies presents an important opportunity, because compared to bi-radicals, their utility is greater for a broader range of materials and biochemical applications, given their smaller size and tunability of chemical property, such as charge, hydrophobicity, hydrophilicity and added functional moieties, as well as the versatility for site-specific functionalization and targeted adsorption. Therefore, it is highly desirable and consequential to enhance and optimize the ssDNP performance of mono-radicals

with an improved mechanistic understanding. This is an alternative to the currently popular approaches that focus on designing optimal bi-radical architectures[15,16,24], and is driven by the necessity to exploit selectively adsorbing or functionalizable mono-nitroxide probes for the study of contemporary functional materials. These include the usage of TEMPO or S-(2,2,5,5-tetramethyl-2,5-dihydro-1H-pyrrol-3-yl)methyl methanesulfonothioate (MTSL) derivatives that is the modus operandi for EPR-based characterization approaches. For example, the wide commercial availability of mono-nitroxide derivatives, such as 4-Amino TEMPO, 4-Carboxy TEMPO, 4-Hydroxy TEMPO, etc. permits the use of a wide range of chemical reactions that can attach the mono-nitroxide spin labels to proteins, gels or soft materials, while they can also be imbibed into porous functional materials with different affinities for surface adsorption, depending on their charge, size and chemical moiety, for the purpose of selective characterization of the local region surrounding the spin probe. Comparatively, in the case of bi-radicals, tuning these properties require synthesis of a new bi-radical for each desired attribute, which can be challenging or infeasible.

The experimental condition relevant to this study is DNP operation at liquid helium temperatures (4-40 K), which yields an entirely different range of relaxation times compared to liquid nitrogen temperatures between 80-150 K that is the most common operating condition for magic angle spinning (MAS) ssDNP employing gyrotron sources[25–30]. Qualitatively, the ability to saturate the electron spin system increases with decreasing temperature, as T_{1e} generally lengthens. The electron spin relaxation timescales, for example T_{1e}, increase by up to 2 orders of magnitude to $O(10^1\text{-}10^2$ ms) at 4 K compared to $O(10^0$ ms) at > 90 K temperatures for nitroxide radical species, whose exact values depend on the electron spin concentration. This permits the use of μw sources that output significantly lower power than gyrotrons when operating at temperatures below 40 K, such as solid-state μw sources, while still yielding high levels of signal enhancements and absolute nuclear spin polarization[10,11,18]. Solid-state sources offer unique benefits, such as a wide tuning range spanning > 10 GHz, phase stability and programmability.

Here, we present a study of static DNP performance of the mono-radical, 4-Amino TEMPO (4AT), and the bi-radical, TOTAPOL in a frozen water:glycerol solution at 4 K and 7 T. To gain a more in-depth mechanistic understanding of the ssDNP process under the present experimental conditions, we compare the DNP efficiency, μw frequency dependence and build-up time constant with a set of electron and nuclear spin relaxation parameters. In order to study the influence of electron spin relaxation and the inter-radical distance on the DNP performance, we varied the radical concentration, while keeping the temperature constant. Our studies demonstrate the importance of electron spin dynamics timescales in tuning the DNP performance, based on their effects on determining the steady-state saturation / excitation profile of the EPR spectrum of nitroxide radicals that is inhomogeneously broadened and span $O(10^2\text{-}10^3$ MHz) in the solid state at 7-9 T. The saturation / excitation profile of an inhomogeneously broadened EPR spectrum depends on the employed μw power, as well as the electron spin lattice relaxation time, T_{1e}, the electron spin dephasing time, T_M, and the spectral diffusion time, T_{SD}, all timescales of which are dependent, to a varying degree, on the magnetic field, temperature and the spatial distribution of the electron spins[31,32]. Most importantly, we define an *integral EPR saturation factor* of the nitroxide spectrum that should be thought of as the 'area under the curve' for the saturation of an inhomogeneously broadened line, as derived from the product of T_{1e} and the electron spin flip-flop rate, W', whereby W' is extracted from the temperature dependence of T_M and is related to T_{SD}. The experimental determination of these relaxation parameters and their suggested roles will be discussed in detail. The essence of our result is that comparable nuclear

spin polarization (P_n) can be obtained with 4AT and TOTAPOL radicals, which is reconciled with a comparable integral EPR saturation factor observed. Surprisingly, the largest P_n is observed at an intermediate spin concentration for both the mono- and bi-radicals, which is rationalized by introducing the framework of an optimum integral EPR saturation factor for tuning the CE DNP efficiency, as will be carefully laid out in this study.

2. Experimental Section

Sample preparation

A solid powder of 4-AT (Sigma Aldrich) radical was dissolved in a solution mixture with a 5:4:1 volume ratio of d-glycerol:D_2O:H_2O and diluted to produce a solution containing 1.7-40 mM nitroxide radicals. TOTAPOL (DyNuPol) is prepared in the same manner. 40 µL of the nitroxide solution is then pipetted into a 7 mm outer diameter and height, 6 mm inner diameter cylindrical teflon sample cup custom-made for our home-built 300 MHz NMR probe[18]. The sample is placed into this cup and cooled down to 4 K inside a custom Janis STVP-NMR cryostat operating in continuous-flow mode.

Solid state DNP and NMR measurement

The key hardware components needed for the high-field 200 GHz DNP operation have been described in detail in previous publications[18,33]. Crucially, the µw system consists of a low power (50-70 mW), frequency tunable, diode-based source (Virginia Diodes Inc.), and a quasi-optical µw bridge (Thomas Keating Ltd.) for transmitting the µw with minimal loss into a corrugated waveguide placed inside a 7 T superconducting magnet (Bruker Biospin). Installed at the end of the corrugated waveguide, at the sweet spot of the magnet, is the NMR probe consisting of an Alderman-Grant ^{1}H NMR coil enclosing the sample and a silver mirror placed below the sample to reflect unabsorbed µw back to the sample. The entire corrugated waveguide and NMR probe is placed inside a custom-designed Janis STVP-NMR cryostat that can be operated at temperatures of 3 K and above. All DNP experiments presented here were performed at 4 K and at 7 T, and using a 300 MHz ^{1}H NMR rf frequency channel of a Bruker 300 Avance solution-state NMR spectrometer. A standard saturation-recovery pulse sequence ending with a solid echo detection was used to measure the recovery time of ^{1}H magnetization to its thermal equilibrium value in the absence of µw irradiation, i.e. the spin-lattice relaxation timescale, T_{1n}, as well as the buildup timescale of the DNP signal upon application of µw irradiation, T_{DNP}, for all experiments. After a certain recovery delay, t, the recovered NMR or built up DNP signal was detected with a solid echo pulse sequence (90_x-τ-90_y) with an inter-pulse delay, τ. Both T_{1n} and T_{DNP} values were obtained using a single exponential fit to the saturation recovery curve,

$$M_z(t) = M_\infty[1 - \exp(-\frac{t}{T_j})]$$, where T_j is either T_{DNP} (µw on) or T_{1n} (µw off). A long interpulse

spacing (τ = 200 µs) was used for the solid-echo detection sequence in all experiments to filter out spurious background signals that have short transverse relaxation timescales (T_{2n}) of about 32 µs, compared to 119 µs for all samples.

A ssDNP frequency profile is obtained by measuring the NMR signal enhancements, $\varepsilon(v)$, at different µw irradiation frequencies (v) at a given signal build up/magnetization recovery (t = 150 s in our case), as presented in Figure 1. The value for $\varepsilon(v)$ is quantified by taking the ratio of the area of the NMR signal with (S_{DNP}) and without (S_{NMR}) µw irradiation [$\varepsilon(v) = S_{DNP}/S_{NMR}$]. Since T_{1n} (spin-lattice relaxation) > T_{DNP} (DNP buildup), the enhancement value has to be adjusted to its steady state value (at t = ∞) by extrapolating the enhancement value using the T_{1n} and T_{DNP} values for the exponential magnetization recovery or buildup. At all concentrations, T_{DNP} is measured at the µw frequency where the maximum positive NMR signal enhancement is found. Thus, S_{DNP} and S_{NMR} are extrapolated to $S_{DNP,\infty}$ and $S_{NMR,\infty}$ before taking the ratio to arrive at the equilibrium DNP enhancement value of $\varepsilon_\infty = S_{DNP,\infty} / S_{NMR,\infty}$. From the ε_∞ values, the extrapolated maximum % nuclear polarization, P_∞, can be obtained by multiplying ε_∞ with the thermal equilibrium % spin polarization at 4 K and 7 T.

Electron paramagnetic resonance (EPR) at 8.5 T

Continuous wave (cw) and pulsed EPR measurements were carried out at 240 GHz using a low power (~30-50 mW) solid state source, developed as the staging instrument for a Free Electron Laser-powered EPR spectrometer[34]. It operates similarly to other high-field pulsed EPR spectrometers reported on in the literature that utilize a low power source, a quasi-optical bridge and induction-mode, superheterodyne, detection[35,36]. Sample volumes of 5 to 10 µL were placed in a Teflon sample cup with a ~3.5 mm inner diameter and 5 mm height, and loaded into the waveguide that is placed in a custom Janis STVP-NMR continuous-flow cryostat pre-cooled to 230 K.

Echo-detected spectra were measured by recording the integrated echo area on a digital oscilloscope (Lecroy Corporation DDA-120) as the superconducting sweep coil (separate from the magnet's main coil) is swept through resonance. The maximum power (~30 mW) available from the solid state source was employed for a 650 ns- τ -750 ns- τ spin-echo pulse sequence, where the pulse lengths were chosen empirically to give the best echo intensity and shape.

The same pulse sequence was used in measurements of the phase-memory times (T_M), at the magnetic field that yielded the maximum echo intensity for the 4-AT or TOTAPOL spectrum. The resulting echo decay was fit with a stretched exponential decay $\exp(-2\tau/T_M)^\alpha$, whereby α = 3/2 was empirically chosen and verified for a frozen glycerol-water glass nitroxide sample system[37]. The uncertainties in T_M are estimated as ±5% of the measured values from repeated measurements.

Measurements of the electron spin-lattice relaxation times (T_{1e}) were carried out with a 3-pulse saturation sequence of the form: saturation-T-650 ns- τ -750 ns- τ. Where T is the recovery delay and τ is the inter-pulse delay. The saturation pulse length was varied until no change in the signal buildup was observed by lengthening the saturation pulse, which ranged from 10 to several hundred milliseconds. The experimental curves were fit by a bi-exponential buildup of the form, $y = y_0[1 - A\exp(-\dfrac{t}{T_{SD}}) - B\exp(-\dfrac{t}{T_{1e}})]$, where T_{SD} is the faster time constant corresponding to the spectral diffusion process and T_{1e} the slower time constant[31].

3. Results and Discussion

DNP mechanism

The ssDNP process has been described in the literature to occur via one or a combination of three main mechanisms, namely the solid effect (SE), cross effect (CE) and thermal mixing (TM) mechanisms[38–46]. These mechanisms rely, respectively, on the interaction between isolated electron-nuclear (*e-n*) spins, three spins of an electron-electron-nuclear (*e-e-n*) coupled system, or networks of many electron and nuclear spins. The bi-radical TOTAPOL was designed with the aim of promoting the *e-e-n* interactions responsible for the CE mechanism, by bringing two radicals close together (1.3 nm)[14] to increase their dipolar coupling, so that the mutual flip-flop of the strongly dipolar coupled electron spin pairs would drive the spin flip of a nearby nuclear spin. The CE condition for this concerted *e-e-n* flip-flop-flip process is fulfilled when the nuclear Larmor frequency is matched by the frequency difference between the dipolar-coupled electron spin pair, whose frequency is spanned by the nitroxide radical's large *g*-anisotropy. The mono-radical may follow one or a combination of the three DNP mechanisms, depending on the radical concentration that tunes the *e-e* distance distribution.

As outlined in the introduction, the DNP mechanism greatly depends on the spatial distribution of radicals. While the average inter-molecular distance, r_{inter}, can be readily modified by the molecular concentration, C_{mol}, the bi-radical intra-molecular distance, r_{intra}, remains fixed. Information about the DNP mechanism can be inferred from the shape of the DNP frequency profile[10,47], where the DNP-driven NMR signal enhancement is plotted against the µw irradiation frequency. Representative DNP profiles of a frozen glass of 4-AT solution at 1.7 and 20 mM concentrations, as measured at 7 T, are shown in Figure 1. The DNP profile has two extrema, which arise from a spin energy transfer from the radicals to nuclear spins that result in a maximum net population of the spin-up (↑) or spin-down (↓) nuclear spin states, yielding positive and negative ssDNP enhancements, respectively. The span of these extrema is denoted as Δ_{DNP}. Changes in the dominant DNP mechanism, especially between the SE and the CE or TM mechanism, will be reflected in changes to the Δ_{DNP} values[10,47]. The Δ_{DNP} values are determined from experimental DNP frequency profiles (such as those shown in Figure 1) and are summarized in Table 1. The first step in evaluating the DNP mechanism is to compare the Δ_{DNP} values to twice the nuclear Larmor frequency, $2\omega_n$, as well as the inhomogeneously broadened EPR spectrum. If $\Delta_{DNP} = 2\omega_n$ and the DNP frequency profile presents enhancement maxima outside the frequency range of the EPR spectrum, the SE mechanism (*e-n* interaction) is the dominant mechanism. Conversely, if $\Delta_{DNP} \neq 2\omega_n$ and the DNP enhancement maxima lie within the EPR spectral density where dipolar coupling between multiple electrons are more likely, the CE (*e-e-n* interaction) and/or the TM mechanism (multi *e-n* interaction) is expected to be the dominant mechanism. In order to illustrate these differences, a representative, echo-detected, EPR spectrum of 20 mM 4-AT is shown above the experimental DNP frequency profiles in Figure 1. The EPR spectra for all other mono- and bi-radical concentrations are included in the supporting information, since they do not vary significantly (~50 MHz) compared to the width of their EPR spectra (base-to-base width ~ 1.1 GHz). To assist in the following discussion, r_{inter} will be given in parenthesis along with C_{mol}, while r_{intra} of TOTAPOL is fixed at 1.3 nm. Referring to Table 1, Δ_{DNP} for 4-AT narrows from 500 MHz to 300 MHz when C_{mol} drops from 40 mM (1.9 nm) to 20 mM (2.4 nm), and starts to broaden again to 350 MHz at 10 mM (3.0 nm), and to 600 MHz at 1.7 mM (5.5 nm). In contrast, Δ_{DNP} remains at 400 MHz for the TOTAPOL sample at 5

and 10 mM concentrations (r_{intra} = 1.3 nm, r_{inter} = 3.8 and 3.0 nm), and is broadened to 550 MHz only at 20 mM (r_{intra} = 1.3 nm, r_{inter} = 2.4 nm). Taken together, we observe that Δ_{DNP} is invariant at 5 and 10 mM TOTAPOL concentrations whereas Δ_{DNP} varies with each 4AT concentration, indicating that the DNP mechanism of the bi-radical only becomes sensitive to inter-molecular effects at C_{mol} > 10 mM (r_{inter} < 3.0 nm), but is governed mainly by the e-e dipolar coupling given by the value of r_{intra} at C_{mol} < 20 mM. More importantly, $\Delta_{DNP} \neq 2\omega_n$ for both radical species (such as profile in black trace, closed symbol, in Fig.1), except for 1.7 mM 4-AT for which we observe $\Delta_{DNP} = 2\omega_n = 600$ MHz (see profile in red trace, open symbol, in Fig.1). All enhancement extrema lie within the EPR spectral density (Fig.1). From these observations we can conclude that the TM and/or CE mechanisms dominate for samples with $C_{mol} \geq 5$ mM ($r_{inter} \leq 3.8$ nm), while the SE mechanism only becomes important at lower C_{mol}, and dominates at 1.7 mM. Whether the CE or the TM mechanism or a mixture of these two mechanisms are effective is a debated question in the DNP literature, although the studies by Shimon *et al.*[10] and Banerjee *et al.*[47] show that a mixed SE and CE model can be sufficient to model the experimentally obtained DNP profiles at 3.4 T for similar samples of nitroxide radicals as used in this study. This does not necessarily exclude possible mixed effects from TM. However, the radical concentration dependence of our DNP result will ultimately show that a dominant CE mechanism is highly likely for the samples studied here at spin concentrations above 5 mM.
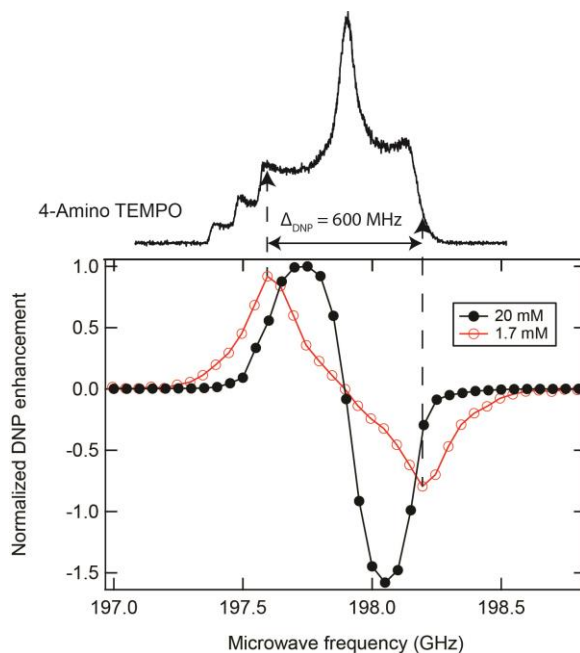

Figure 1 Representative echo-detected EPR spectrum and DNP frequency profiles of 4-AT at 1.7 mM (open red symbol) and 20 mM (closed black symbol) concentrations. The lines between data points are drawn to guide the eye. Each curve is normalized to the maximum enhancement of the left peak, which would correspond to the maximum positive enhancement. Since the EPR spectra do not vary significantly between different concentrations and radical types, a representative EPR spectrum of 20 mM 4-AT is included at the top of the figure to help visualize the overlap between the span of the DNP frequency profile and the EPR spectrum. The x-axis of the EPR spectrum shown here is equivalent to the x-axis of the DNP frequency profile, after linearly scaling to 7 T from the 8.5 T field employed for EPR (spectra shown in Figure S1). The dotted lines that span the maxima of the DNP profile of the 1.7 mM 4-AT sample corresponds to a value equalling $2\omega_n$ that is the Δ_{DNP} width expected for the SE mechanism.

The effect of inter-molecular vs. intra-molecular electron spin interactions on the DNP mechanism observed earlier can be explained by considering the concentration dependence of electron spin dipolar coupling that arises from the proportionality of dipolar coupling to the *e-e* distances, r_{intra} and r_{inter}. The nearest neighbor distance distribution for the mono-radical is given by (and plotted in Figure 2)[48]:

$$w(r) = 4\pi r^2 n \exp\left(-\frac{4\pi r^3 n}{3}\right)$$

(1)

where $r = r_{\text{inter}}$, n = number of particles/volume and $w(r)dr$ is the probability of finding particles within dr. From Figure 2, one can see that the distribution of r_{inter} for mono-radicals narrows and averages at smaller values at high radical concentrations, whereas at low radical concentrations, r_{inter} has a broader distance distribution around a higher average value for r_{inter}. This distance distribution obviously changes much less sensitively when lowering the bi-radical molecular concentration, as the nearest neighbor distance is unaltered. This means at higher radical concentrations, there is a higher probability for either mono- or bi-radicals to find a nearby electron spins to experience high *e-e* dipolar coupling, while lowering the radical concentration will reduce this probability significantly stronger for the mono-radicals since it directly affects their nearest neighbor distance distribution. For example, compared to the fixed bi-radical $r_{\text{intra}} = 1.3 \pm 0.1$ nm, only 7 % of electron spins of a mono-radical have $r_{\text{inter}} \leq 1.4$ nm at 10 mM, while this population increases to 24 % at 40 mM concentrations. This is reflected in our data in the invariance of Δ_{DNP} at 5 and 10 mM TOTAPOL concentrations, which indicates that the DNP mechanism of the bi-radical only becomes sensitive to inter-molecular effects at $C_{\text{mol}} > 10$ mM ($r_{\text{inter}} < 3.0$ nm), but is governed mainly by the *e-e* dipolar coupling resulting from r_{intra} at $C_{\text{mol}} < 20$ mM. In contrast, Δ_{DNP} changes with every mono-radical concentration tested, which directly tweaks the nearest neighbor *e-e* distance that is thought to be responsible for determining the dominant DNP mechanism, by changing the strongest contributors to the *e-e* dipolar coupling.
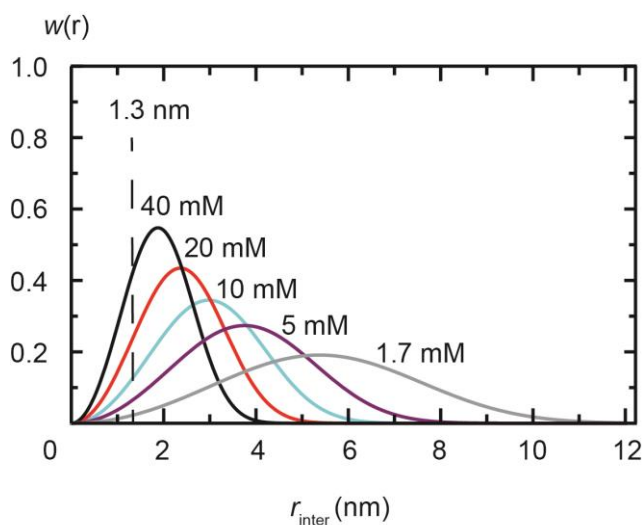
Figure 2 Theoretical next-nearest neighbour distance distribution (r_{inter}) for mono-radicals calculated from Equation 1

DNP-induced nuclear spin polarization

While there are distinct differences observed in the dependence of Δ_{DNP} on the spin probe's molecular concentration (C_{mol}), we observe that mono- and bi-radicals exhibit similar P_n as a function of spin concentration. Here, P_n is analyzed with respect to the spin concentration per unit volume, C_{spin}, whereby $C_{spin} = 2C_{mol}$ for the bi-radical. Figure 3 shows that P_n follows the same C_{spin} dependence for both mono- and bi-radicals with an optimum C_{spin} found at 20 mM, yielding P_n values of 29 % and 24 % for TOTAPOL and 4-AT, respectively. Thus, at the optimum $C_{spin} = 20$ mM, the value of P_n for TOTAPOL only exceeds that of 4-AT by a factor of 1.2. This has to be compared to earlier literature studies, which obtained a factor of > 5 using MAS-DNP at 90 K and > 5 T[15]. This indicates that, under the present conditions (static DNP, 4 K and 7 T), the fixed intra-molecular distance of the TOTAPOL bi-radicals provides a much less significant advantage over 4-AT mono-radicals than observed earlier at 90 K (e.g. see Ref. [15]).
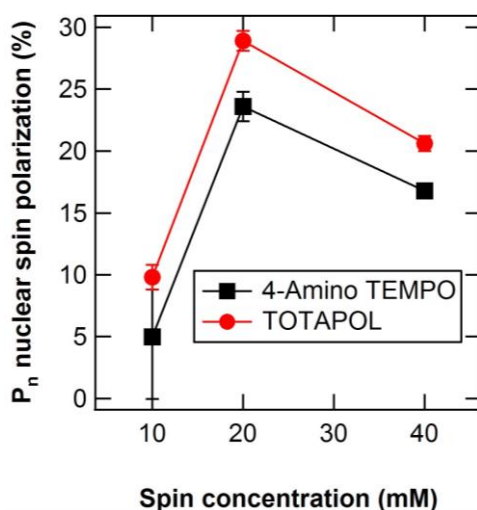
Figure 3 DNP-induced nuclear spin polarization as a function of spin concentration. The nuclear spin polarization for 10 mM 4-AT at steady state cannot be determined but the upper limit is calculated to be 11 % based on the enhancement at 150 s. Lines are drawn between points to guide the eye.

For both mono- and bi-radicals, the rise in P_n when increasing spin concentration from 10 to 20 mM can be rationalized with a higher probability of finding electron spin pairs exhibiting a frequency spacing of 300 MHz, given stronger dipolar coupling. However, the similarity in P_n between the mono- and bi-radicals at 4 K is peculiar since the bi-radicals obviously experience a higher overall dipolar coupling at these lower concentrations.

We make another unexpected observation, namely that further increasing the spin concentration from 20 to 40 mM results in a drop in P_n for both radical species. This effect cannot be explained in terms of radical distribution and the increasing dipolar coupling, since both factors should further enhance the DNP performance in the CE regime. Thus, other parameters that determine DNP performance such as electron and nuclear spin relaxation must be considered, as will be outlined next.

Effect of spin relaxation on nuclear spin polarization

Besides the strength of the *e-e* dipolar coupling and the spatial radical distribution, important factors that influence P_n are the nuclear and electron spin relaxation times. They determine to what extent the EPR spectrum can be saturated and how efficiently electron spin polarization can be transferred to nuclear spins. For example, the saturation factor of a homogeneous EPR spectrum is proportional to T_{1e} x T_{2e}, which has been suggested to correlate with P_n for different bi-radical configurations[16], where it was assumed that $T_{2e} = T_M$. However, this expression is not applicable to a nitroxide EPR spectrum that is inhomogeneously broadened. In contrast to a homogeneous EPR spectrum, an inhomogeneously broadened EPR spectrum contains a large number of spin packets. In the simplest case those spin packets are independent, and applying a continuous µw irradiation burns a narrow hole into the spectrum. In such a case only a very small part of the EPR spectrum is saturated while the remaining part is not excited. In order to saturate more than one of these spin packets, it is necessary that spin packets are connected through dipolar coupling, such that the excitation can be propagated among spin packets by electron spin flip-flops. This effect is referred to as spectral diffusion, with a characteristic time constant. In the presence of strong spectral diffusion, the hole, which is burnt into the EPR spectrum by microwave excitation, will widen. As a consequence more electron spin packets in the EPR spectrum will be saturated and P_n may be enhanced. Hence, for an understanding of the DNP performance, knowledge about the saturation of an inhomogeneously broadened EPR spectrum is mandatory.

Spectral diffusion influences both the saturation recovery experiment that determines T_{1e} and electron spin echo measurements that determines T_M. When the spectral diffusion time constant is determined from saturation recovery experiments following $y = y_0[1 - A\exp(-t/T_{SD}) - (1-A)\exp(-t/T_{1e})]$ [31] (section), the T_{SD} value obtained is convoluted with spin relaxation effects of the given radical system, as it is extracted from the fast component of the bi-exponential saturation recovery curve. Thus, T_{SD} alone cannot quantify the amount of EPR saturation without simulating the specific effect of spectral diffusion on a nitroxide EPR spectrum, as previously attempted by Thurber *et al.* using Bloch equations[11]. Fundamentally, the spectral diffusion rate determined here is governed by *e-e* flip-flop processes, characterized by a flip-flop rate, W. Crucially, we have an alternative experimental technique at our disposal to directly determine a quantity very close to W, that is not affected by T_{1e}, namely the flip-flop rate of the majority of the unexcited EPR spins, W', from T_M measurements across different temperatures well above to near or below the Zeeman temperature (T_Z) of 11.5 K at 8.5 T (see Figure S2). This analysis method relying on the so called spin bath quenching effect has been previously developed by Takahashi et al.[49], and was subsequently applied to solutions of 4-Amino TEMPO in glycerol:water mixture.[37] The same process to determine W' is exploited here (supporting information).

In order to assess the area of the hole caused by µw irradiation (see Figure 5), we introduce an empirical integral saturation factor $s_{int} = T_{1e} \times W'$, which takes into account the combined effect of spin-lattice relaxation and spectral diffusion that proceeds by electron spin flip-flops. When applying a continuous µw irradiation to an inhomogeneously broadened EPR spectrum of nitroxide-based radicals, the width of this hole will depend on T_{1e} and W', as well as the µw power. So, in order to evaluate the integral saturation factor for different sample systems, T_{1e}, T_{SD} at the temperature of the DNP experiment, T_M as a function of temperature above to below T_Z, and W from this temperature dependent T_M curve, must be determined. As outlined in section

2, these parameters were determined by pulsed EPR measurements at 8.5 T. The values are presented in Table 1 along with parameters characterizing the DNP performance and plotted in Figure 4 as a function of spin concentration. A general trend found for the nuclear and electron spin relaxation timescales, as presented in Figure 4, is a monotonic decrease in electron (Figure 4a, b, e and f) and nuclear (Figure 4c and d) spin relaxation times (or increase in spin relaxation rates) with increasing radical concentration. This is because all of these spin relaxation timescales are modulated by the $e\text{-}e$ dipolar coupling between the radicals, or by the $e\text{-}n$ dipolar coupling between the radical and the solvent nuclei. The relaxation time constants are therefore directly affected by the radical concentration. As expected, T_{1e} and T_M decrease with increasing mono- and bi-radical concentration (Figure 4a and b). This is because increasing radical concentration increases the $e\text{-}e$ dipolar coupling, which enhances the flip-flop rate of the electron spins, resulting in the observed decrease in T_M. The connection between $e\text{-}e$ dipolar coupling and T_{1e} is less obvious, but previous studies by Sato *et al.*[50] observed that dipolar interactions at $e\text{-}e$ distances below 1 nm are responsible for the decrease in both T_{1e} and T_M with increasing radical concentration. Although the average r_{inter} and r_{intra} are above 1 nm for the mono- and bi-radical concentrations employed here, the plot of the nearest neighbor distance distribution in Figure 2 reveals that there are non-negligible populations of electron spins that possess r_{inter} below 1 nm at all radical concentrations studied here.
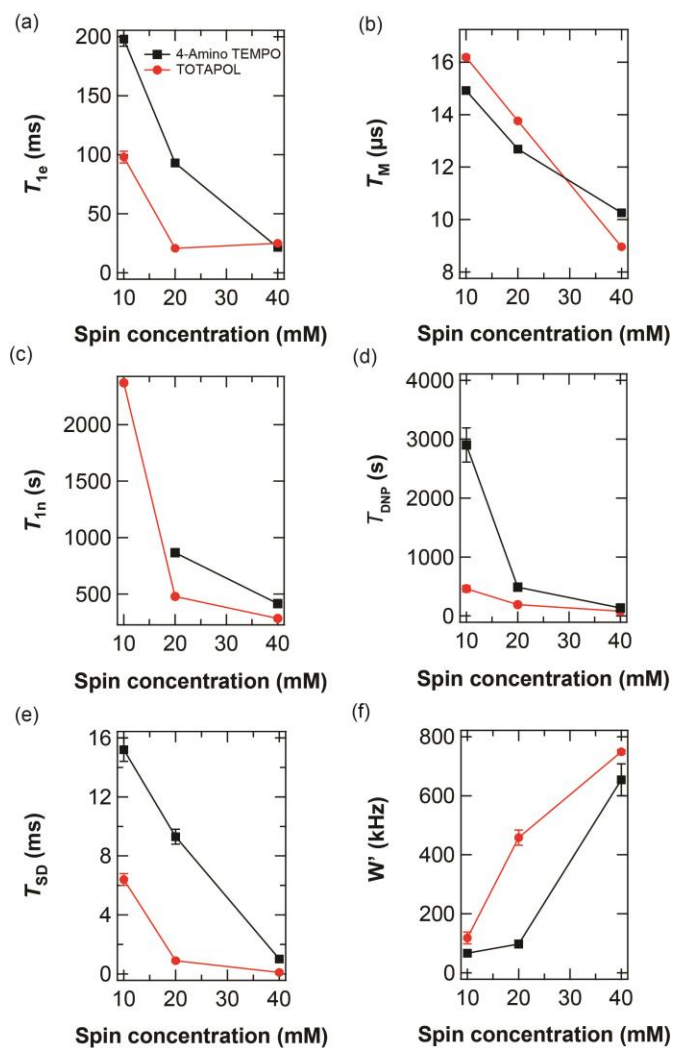
Figure 4 Plot of spin relaxation timescales (a) T_{1e}, (b) T_M, (c) T_{1n}, (d) T_{DNP}, (e) T_{SD}, and (f) W' vs. C_{spin}, as reported in Table 1 and 2. The lines are drawn to guide the eye.

Table 1 7 T % nuclear polarization (P_n), peak-to-peak DNP frequency width (Δ_{DNP}), nuclear (T_{1n}, T_{DNP}) relaxation timescales, and 8.5 T electron (T_{1e}, T_M) relaxation timescales at 4 K. The concentration dependence of the spin relaxation timescales shown below in this table is plotted in Figure 4. The electron spin relaxation timescales, T_{1e} and T_M, were measured at 8.5 T, while the NMR and DNP measurements were performed at 7 T. The electron spin polarization differs by only 6 % between 7 T (83 %) and 8.5 T (89 %) at 4 K, so that the trends in the EPR parameters at 8.5 T that result from changes in radical concentration should remain similar to that at 7 T.

Composition	Δ_{DNP} (MHz)	ε_∞ / P_n	T_{1e} (ms)	T_M (µs)	T_{DNP} (s)	T_{1n} (s)
40 mM 4-AT	500	93 ± 3 / 16.8 ± 0.5	21.5 ± 0.2	10.26 ± 0.04	135 ± 8	416 ± 52
20 mM 4-AT	300	131 ± 7/ 23.6 ± 1.2	93 ± 3	12.69 ± 0.04	487 ± 18	866 ± 103
10 mM 4-AT	350	64/ 0.18 $<P_n< 11$	198 ± 6	14.92 ± 0.05	2901 ± 292	> 3000
1.7 mM 4-AT	600	~12 / -	-	-	-	-
20 mM TOTAPOL	550	114 ± 3 / 20.6 ± 0.6	25 ± 1	8.96 ± 0.03	80 ± 5	284 ± 13
10 mM TOTAPOL	400	161 ± 5/ 28.9 ± 0.8	20.8 ± 0.2	13.76 ± 0.05	190 ± 6	478 ± 31
5 mM TOTAPOL	400	54 ± 6/ 9.8 ± 1.0	98 ± 5	16.19 ± 0.08	460 ± 52	2371 ± 278

We find corroborating experimental support that the flip-flop process presented here with the rate, W', fundamentally underlies the spectral diffusion process characterized by, T_{SD}, with the observation of an inverse and monotonic relationship between T_{SD} and W', as presented in Figure 6a. Still, they are not equivalent quantities, given the stronger influence from spin relaxation effects on T_{SD}. Interestingly, these T_{SD} vs. W' curves entirely overlap for the TOTAPOL and 4-AT samples, implying that the governing relationship between spin flip-flop and spectral diffusion processes is the same for the mono- and bi-radical system.

The experimental values for T_{SD} and W' are recorded in **Table 2**, where it can be seen that the bi-radical possesses a much larger W' and faster T_{SD} values compared to the mono-radical at a given C_{spin} (Figure 4e and f). This indicates that the bi-radical architecture significantly enhances the e-e flip flop rate of unexcited electron spins, which can be explained by a larger dipolar coupling of the nearest neighbor electron spin of the bi-radical compared to the mono-radicals. For both radical species, the increase in radical concentration increases the overall e-e dipolar coupling, enhancing the e-e flip-flop process, thereby increasing W' and decreasing T_{SD}.
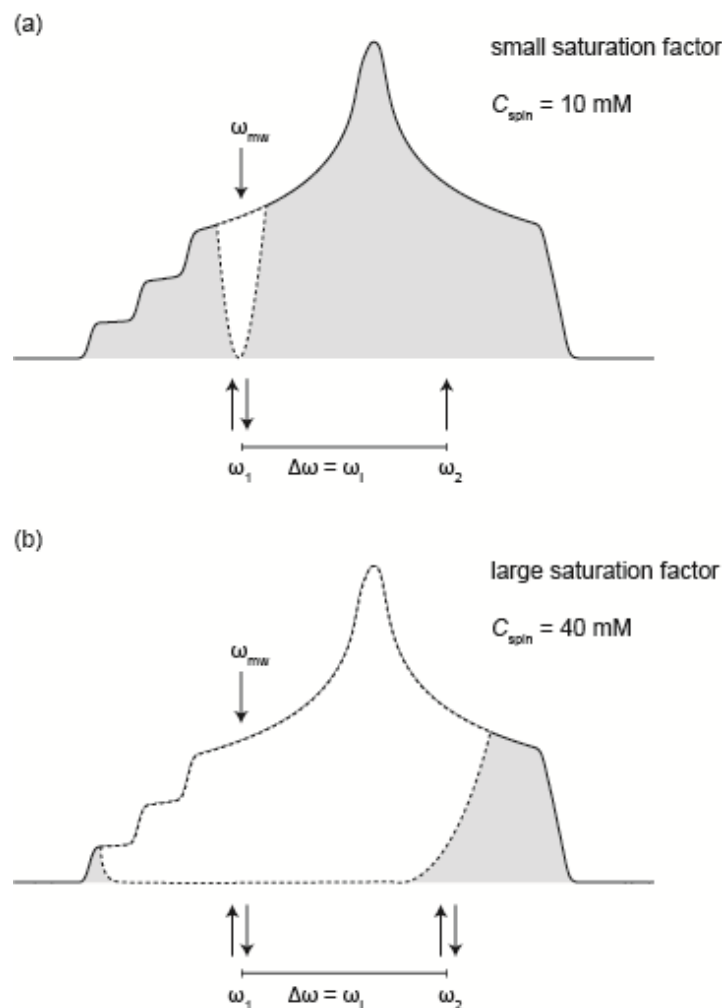
Figure 5 Pictorial representation of what we refer to the "area under the curve" that defines the integral saturation factor, s_{int}, of an inhomogeneously broaded solid-state EPR spectrum of nitroxide radical. Illustrated is the effect of a (a) small integral saturation, as found for $C_{spin} = 10$ and (b) large integral saturation, as found for $C_{spin} = 40$ mM samples.

Having established the basis for defining an integral saturation factor for an inhomogeneously broadened spectrum, we can now compare s_{int} for the different samples at different spin concentration (s_{int} as a function of C_{spin} is shown in Figure 6b). As can be seen from Figure 6b, the product of T_{1e} and W' that determines s_{int} is comparable for the two radicals at equal C_{spin}. Specifically, when evaluating T_{1e} and W' for TOTAPOL and 4-AT at the same C_{spin}, one can see that at C_{spin} values of 10, 20 and 40 mM, T_{1e} decreases by a factor of 0.86 ± 0.04, 4.5 ± 0.2 and 2.0 ± 0.1 from 4-AT to TOTAPOL. This is balanced by the increase in W' by a factor of 1.2 ± 0.1, 4.7 ± 0.7 and 1.8 ± 0.4 from 4-AT to TOTAPOL. Hence, the shorter T_{1e} but larger W' of the bi-radical architecture results in a shallower but wider EPR saturation profile. The opposite is true for the mono-radical, where its longer T_{1e} values and smaller W' result in a deeper but narrower EPR saturation profile. The opposing changes in T_{1e} and W' between the mono- and bi-radical balance out, serendipitously, to a comparable s_{int} (Figure 5b). This means that a comparable number of electron spins participate in the DNP process. We therefore

hypothesize that the surprisingly similar performance between mono- and bi-radicals (Figure 3) can be explained by the trend for the s_{int} values for the two different radical species. The dependence of DNP performance on T_{1e} and W' (and therefore T_{SD}), however, also implies that the DNP performance will be different under MAS conditions compared to under static conditions, as MAS will affect the spectral diffusion rate during spinning, as observed by Thurber *et al.*[51]
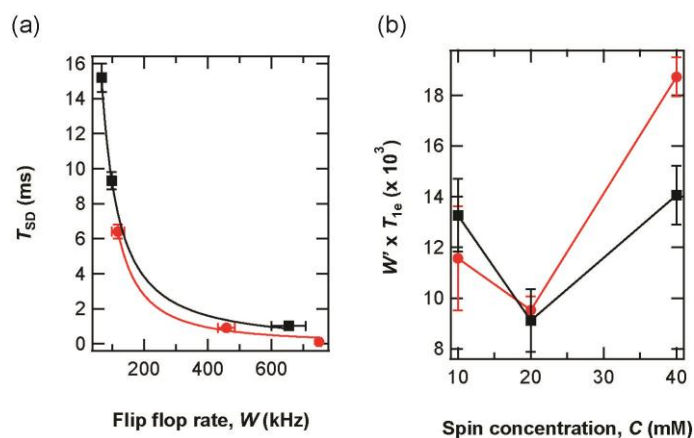
While we can rationalize the comparable P_n for 4-AT and TOTAPOL by a comparable s_{int}, the observation of an optimal C_{spin} to obtain the highest P_n for both radicals is peculiar, especially because s_{int} is found to have a minimum at the most optimal C_{spin}. For this, we need to consider the complex effect of the integral saturation factor on P_n, given that CE DNP relies on upholding an electron spin polarization differential during µw irradiation between the electron pairs that participate in the three-spin flip process, as discussed by Thurber *et al*[52]. The excitation of electron spins at a given µw irradiation frequency from the ↓ to the ↑ state must induce the subsequent flip of dipolar coupled electron spins, at a frequency difference (higher or lower) corresponding to the nuclear Larmor frequency, from the ↑ to the ↓ spin state, in order to induce *e-e-n* spin flip-flip-flops that drive the CE DNP process. This implies there must be an optimum value for s_{int}: if s_{int} is too small (small hole, Figure 5a), an insufficient number of electron spins are excited that can participate and drive the CE DNP process, while if s_{int} is too large (large hole, Figure 5b), the spin polarization difference between the two participating electrons upheld during µw irradiation is smaller, as the ↑ and ↓ spin populations are then equally populated. Recall that 89 % of electron spins are polarized in the ↓ spin state at 8.5 T and 4 K in the absence of µw irradiation. In this scenario, a lower s_{int} can be favorable when the saturation can be so effective that it diminishes the needed electron spin population differential by oversaturation.

In order to further reconcile this mechanism, we have determined the microwave power dependence of P_n. If the smaller P_n observed at the highest radical concentration is indeed due to oversaturation, decreasing µw power under this condition should yield higher P_n. Indeed, this is exactly what we observe: as shown in Figure 7, for the monoradical at $C_{spin} = 40$ mM. P_n first increases as a function of µw power, passes a maximum at 68 mW and then drops sharply. This µw power dependence observed for 40 mM 4-AT is contrasted to that of 20 mM 4-AT, where $P_\%$ continues to increase with increasing µw power, as reported previously[18]. This implies that for 20 mM 4-AT, s_{int} is below the threshold value within the range of µw power available with our DNP experimental setup. Notably, the drop in $P_\%$ from $C_{spin} = 20$ mM to a higher concentration of 40 mM (~7 %) is not as severe as the drop to a lower concentration of 10 mM (~20 %), where the larger $P_\%$ drop can be safely attributed to a lower dipolar energy of the sample system.

The observed trends in P_n as a function of spin concentration and microwave power, also suggest that the observed DNP mechanism is rather the CE. In the framework of the TM DNP mechanism established in the literature[40,41], the larger the value of s_{int}, the more electrons can be excited to establish a spin temperature, and the larger the *e-e* dipolar coupling (i.e. the larger the value of W'), the more electrons can be connected through dipolar coupling to establish a higher (or lower) nuclear spin temperature.

Table 2 Values for T_{SD} and W' at 4 K.

| Molecular concentration, C_{mol} (mM)	Spectral diffusion timescale, T_{SD} (ms)	Flip-flop rate, W' (kHz)
4-AT		
40	1.02 ± 0.04	654 ± 54
20	9.3 ± 0.5	98 ± 13
10	15.2 ± 0.8	67 ± 7
TOTAPOL		
20	0.1 ± 0.1	749 ± 7
10	0.9 ± 0.1	458 ± 26
5	6.4 ± 0.4	118 ± 20

Figure 6 (a) Power law fit of T_{SD} with respect to the *e-e* flip-flop rate, W', for TOTAPOL (●) and 4-AT (■) (c) Product of W' and T_{1e} (s_{int}) with respect to C_{spin}. Lines are drawn to guide the eye.

At the highest radical concentrations, the total dipolar energy, as well as s_{int} for the electron spins is the largest (Figure 6b). Here, the total dipolar energy of the mono-radicals are similar in value to that of the bi-radicals, as exemplified by the narrowing of the distance distribution and decrease in the average values of r_{inter} for the mono-radicals (Figure 2), which leads to the convergence of relaxation values at higher concentrations between both radical species (Figure 4). This indicates that there may not be a clear advantage in terms of the dipolar energy between the mono- and bi-radicals at the high radical concentrations, while both radical systems are subject to oversaturation at this radical concentration, albeit to different degrees. Note that the flip-flop rate, W', amounts to very large values exceeding 600 kHz for both radical species at $C_{spin} = 40$ mM, while T_{1e} is long, on the order of 20 ms, yielding very high s_{int} values.
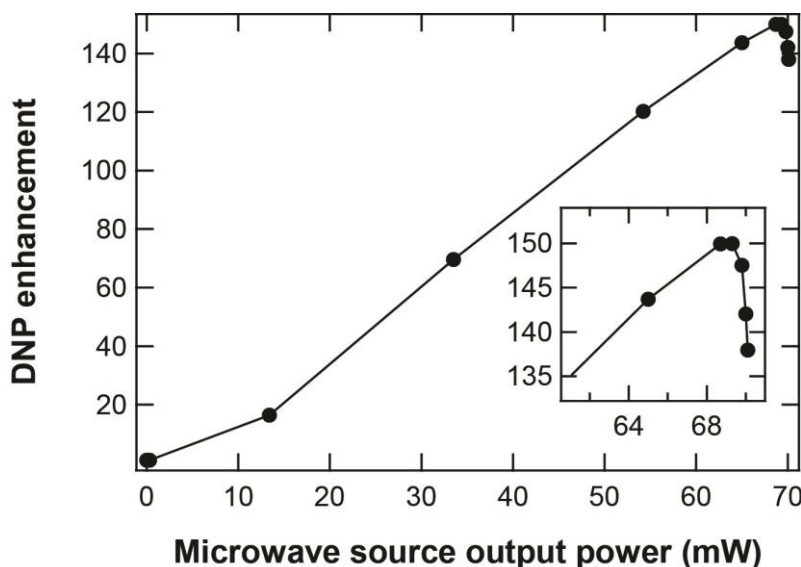
Figure 7 The µw power dependence of DNP enhancement for 40 mM 4-AT. The inset is a zoom-in of the non-linear region of the curve. Lines are drawn to guide the eye.

The observation of an optimum $s_{int,opt}$ value for generating a large P_n implies that the temperature and concentration dependence of spin relaxation timescales such as T_{1e} can be used to modulate the DNP performance under different experimental conditions. This temperature dependence of T_{1e} at 7 T has been experimentally determined, as presented in Figure 8, that illustrates that T_{1e} follows a power law ranging from a proportionality to T^{-1} to as steep as T^{-4}, depending on the radical type and concentration. For the 40 mM 4-AT sample, P_n should increase with temperature up to a threshold temperature, as s_{int} is expected to decrease as T_{1e} moderately decreases with $T^{-1.2}$ (Figure 7a) under over-saturation conditions ($s_{int} > s_{int,opt}$), or at least may not be as sensitively affected with increasing temperatures. In contrast for the 5 mM TOTAPOL sample, P_n is expected to significantly decrease at higher temperatures as T_{1e} decreases more rapidly with $T^{-4.3}$ (Figure 7b), while at under-saturation conditions ($s_{int} < s_{int,opt}$) unless much higher µw powers become available for the DNP experiment. Thus, knowledge of the temperature dependence of spin relaxation times and their effect on DNP performance can be crucial in understanding how to rationally design optimal DNP experimental conditions for specific samples and sample conditions.
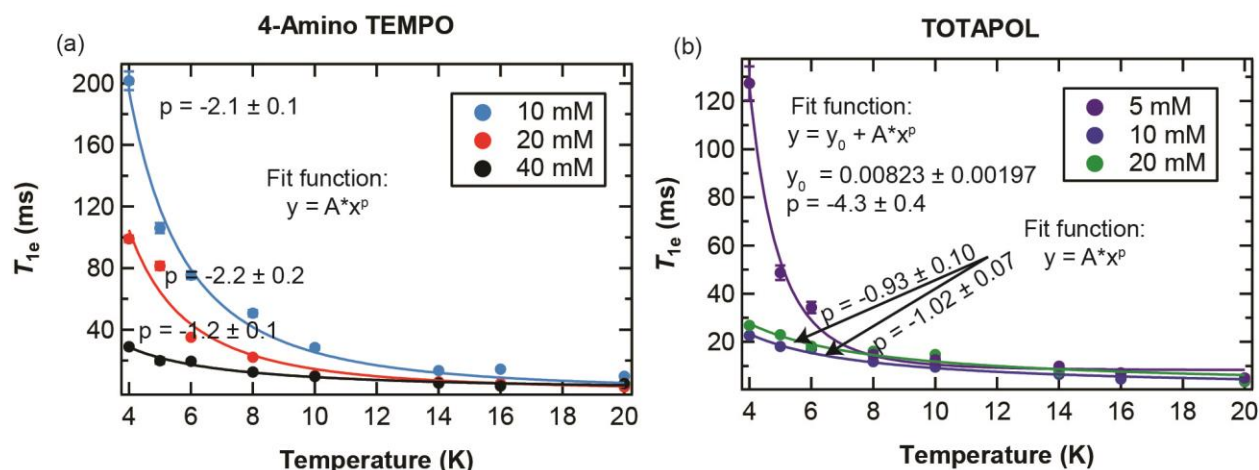
Figure 8 Temperature dependence of T_{1e} for (a) 4-Amino TEMPO and (b) TOTAPOL. Lines are power law fits to the data, with the corresponding equations included in the figure.

*Effect of spin relaxation timescales on T_{DNP}*

Up until now we have only analyzed the maximum nuclear spin polarization that can be achieved by DNP. However, for applying DNP to enhance NMR spectroscopy, it is also of great importance to acquire a nuclear polarization within a reasonable time. As outlined in section 2, the nuclear spin polarization buildup under µw irradiation is mono-exponential with a time constant T_{DNP}, and the DNP performance can be quantified by the maximum nuclear polarization, P_n, over T_{DNP}. In most solid-state DNP studies conducted at temperatures above 90 K, it has been observed that $T_{1n} = T_{DNP}$, which is generally assumed to be the case for all DNP conditions. However, in recent years, Shimon *et al.*[10], Siaw *et al.*[18] and Walker *et al.*[23] have shown that below a certain temperature threshold, the assumption that $T_{1n} = T_{DNP}$ is no longer valid, but rather $T_{DNP} < T_{1n}$ for TEMPOL (4-Hydroxy-TEMPO) in DMSO/water, 4-AT in glycerol/water, or OX063Me trityl in pyruvic acid/glycerol, respectively. However, there has not been a consensus in offering a mechanistic explanation for this observation. With the experimental conditions presented here at 4 K, and for all 4-AT and TOTAPOL concentrations employed in this study, we are well below the temperature threshold for $T_{1n} = T_{DNP}$, with T_{DNP} observed to be always at least a factor of 2 smaller than T_{1n} (Table 1, Figure 4c and d).

This effect can be rationalized in the following way. In a sample containing dispersed paramagnetic radicals, T_{1n} is determined by paramagnetic relaxation due to *e-n* interactions, and thus highly depends on the concentration of paramagnetic radicals. Besides *e-n* interactions, *e-e-n* interactions can also influence T_{1n}[51,53]. For example, two neighboring radicals (such as the neighboring spins in a bi-radical) that possess a large dipolar coupling (~20 MHz for bi-radicals) can undergo a concerted *e-e* flip-flop. When these two electron spins are subject to g-anisotropy, this can easily result in a frequency difference of ~300 MHz, given the $O(10^2$-10^3 MHz) width of the nitroxide spectra at the magnetic fields employed here, to match the ^{1}H nuclear Larmor frequency at 7 T, and thus yielding a nuclear spin flip through a concerted *e-e-n* flip-flop process. The *e-e* dipolar energy alone will not be sufficient to directly match the nuclear Larmor frequency, but it ensures that a concerted two-spin *e-e* flip-flop can be efficiently driven in the first place. This concerted *e-e* flip-flop leads to a flip of the nuclear spin, in the absence of µw irradiation, and is the same underlying process as in CE-DNP. Since the flip of the nuclear spins

occur in a random manner, the *e-e* flip-flop contributes to T_{1n}, if the concentration of paramagnetic radicals is high enough.

Similarly, T_{DNP} is determined by the same processes, i.e. *e-n* and *e-e-n* interactions and is therefore usually equal to T_{1n}. In our case, however, when T_{1n} is measured via a saturation recovery pulse sequence in the absence of μw irradiation, not all *e-n or e-e-n* interactions are activated that drive the CE-DNP processes. Due to the high electron spin polarization (> 80 %) around or below the Zeeman temperature (T_Z), the majority of spontaneous *e-e* spin flip-flops are suppressed unless driven by μw irradiation. We conclude that below a threshold temperature near T_Z, an entirely different mechanism underlies T_{DNP} compared to T_{1n}, where the actively driven and concerted multi-*e-n* spin flip processes dominates the former timescale, while single nuclear spin flip processes facilitated by residual fluctuating dipolar fields from the surrounding electron spins underlie both timescales. It is obvious from the experimental data (Table 1) that the driven multi-*e-n* spin flip process can more efficiently flip nuclear spins per unit time than paramagnetic T_{1n} processes under the experimental conditions employed here, where spontaneous electron spin flip-flops are otherwise suppressed.

In addition to the observation that $T_{DNP} < T_{1n}$, the dependence of nuclear and electron relaxation parameters on C_{spin} show that the relaxation values for mono- and bi-radicals tend to converge at higher radical concentrations, as can be seen in Figure 4. The plots in Figure 4 show that this trend is consistent for both the electron (T_{1e}, T_M, T_{SD} and W') and nuclear (T_{1n} and T_{DNP}) spin relaxation timescales. Interestingly, when plotting T_{DNP} of the mono- and bi-radical against their electron spin relaxation parameters, T_{1e}, T_M, T_{SD} and W' (Figure 9), T_{DNP} for TOTAPOL has the same dependence as 4-AT on every one of the electron spin relaxation times measured here, except for T_M, which only converges at short T_M values. This means that these electron spin relaxation timescales collectively determine the efficiency of the DNP build-up process, as signified by T_{DNP}. The effect of tethering two mono-radicals together is to increase the likelihood that multiple electrons participate in the *e-e* and *e-n* flip-flop process that drives the system towards steady state, effectively generating the same result as increasing the radical concentration. Thus, the electron spin relaxation values are always faster for TOTAPOL at a given C_{spin}, but this fast value falls on the 4-AT curve on a region that reflects a higher C_{spin} value, where the mono- and bi-radical relaxation values converge. Therefore, at higher C_{spin}, even the T_{DNP} vs. T_M curves are expected to converge for the two radical species. One important practical implication of this finding is that, while 4-AT and TOTAPOL at the optimal $C_{spin} = 20$ mM present comparable P_n, T_{DNP} is significantly shorter for TOTAPOL, making it more favorable when considering the gained NMR signal amplitude per unit time.
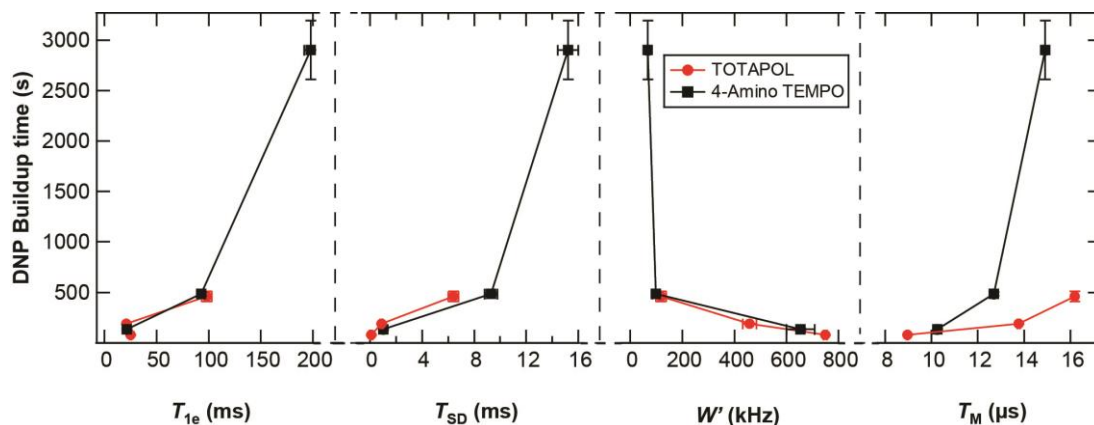
Figure 9 Plot of T_{DNP} vs. relaxation timescales T_{1e}, T_{SD}, W', and T_M. Lines are drawn to guide the eye.

4. Conclusions

In this contribution we investigated the performance of mono- and bi-nitroxide radicals (4-AT and TOTAPOL, respectively) for ^{1}H DNP in a frozen water glycerol solution at a magnetic field of 7 T and a temperature of 4 K. By varying the effective spin concentration, we observe that the DNP frequency profile changes and is also widely different for mono- and bi-radicals. From the DNP frequency profile we conclude that the DNP mechanism shifts from the SE (low concentration) to the CE (high concentration) for the case of monoradicals, while for biradicals the CE prevails for all concentrations investigated. Interestingly, we observe that the nuclear spin polarization obtained by DNP using mono- and biradicals at a specific spin concentration is almost identical. Thus, at the present condition (static DNP, 7T, 4K) bi-radicals do not present a significant advantage over mono-radical. This observation is surprising, since earlier studies, using MAS-DNP at 90 K, reported that biradicals are much more efficient DNP polarizing agents.

Furthermore, P_n first increases as the spin concentration is increased from 10 mM to 20 mM, while it decreases significantly by further increasing the spin concentration to 40 mM. Our observation that P_n exhibits an optimum value at a C_{spin} of 20 mM suggests that an increasing $e\text{-}e$ dipolar coupling as found at higher radical concentrations, i.e. decreasing r_{inter}, does not always lead to an increase in P_n. We therefore conclude that besides the $e\text{-}e$ dipolar coupling, other factors such as electron and nuclear spin relaxation are also important. Thus, the success of TOTAPOL and other designer bi- or tri-radicals does not exclusively originate from ensuring a close $e\text{-}e$ distance with $r_{intra} = 1.3$ nm via the bi-radical architecture to select for a concerted $e\text{-}e\text{-}n$ three-spin flip process that defines the CE DNP mechanism.

Rather, the integral electron spin saturation factor of the inhomogeneously broadened EPR spectrum of nitroxide radicals, s_{int}, defined in this study by the product of T_{1e} and W' is found to be a critical contributor to modulate P_n. Under the experimental conditions employed here, a comparable s_{int} can rationalize the comparable P_n found with 4-AT and TOTAPOL, while an optimal s_{int}, short of oversaturation, can rationalize the optimum P_n found at an intermediate radical concentration of $C_{spin} = 20$ mM for both radical species. We find that a key consequence of the bi-radical architecture is a significant increase in the electron spin flip-flop rate, W', compared to its mono-radical counterpart, that increases the integral EPR saturation factor, s_{int}. If

the temperature and μw power does not result in $s_{int} > s_{int,opt}$ leading to oversaturation as found for $C_{spin} = 40$ mM for 4-AT and TOTAPOL at 4 K, an increase in s_{int} will contribute to higher DNP performance. Thus, a larger s_{int} due to an intrinsically larger W' value can be an added key benefit of the bi-radical architecture compared to the mono-radical counterpart, in addition to the increased electron spin dipolar energy available. However, under experimental conditions where high s_{int} is available, such as at liquid helium temperatures, very high μw power, or combination thereof, this study offers an optimistic perspective for mono-radical species as efficient and competitive DNP polarization agents, especially if the sample and experimental conditions can be deliberately optimized based on the newly refined mechanistic understanding of ssDNP.

The study here also shed light on the observation of $T_{DNP} < T_{1n}$ at liquid helium temperatures in the literature. Due to the high electron polarization at liquid helium temperatures, the *e-e-n* flip-flop process characteristic of the CE DNP mechanism is only activated under μw irradiation, leading to a faster T_{DNP} compared to magnetization recovery through T_{1n} processes. To completely understand the effects of spin relaxation on DNP processes under a broader range of experimental conditions, it will be necessary to analyze the effect of varying spin relaxation on P_n and T_{DNP} at unaltered spin concentration and radical architecture, which requires more extensive studies of the temperature dependence of all DNP and electron spin dynamics parameters. Ultimately, a deeper mechanistic understanding of ssDNP permits the rational design of optimal DNP experiments for a given sample or material of interest.

Acknowledgments

Notes and References

1. O. Lafon, A. S. L. Thankamony, T. Kobayashi, D. Carnevale, V. Vitzthum, I. I. Slowing, K. Kandel, H. Vezin, J.-P. Amoureux, G. Bodenhausen, and M. Pruski, *J. Phys. Chem. C*, 2012, **117**, 1375–1382.

2. D. Lee, H. Takahashi, A. S. L. Thankamony, J.-P. Dacquin, M. Bardet, O. Lafon, and G. De Paëpe, *J. Am. Chem. Soc.*, 2012, **134**, 18491–18494.

3. A. E. Dementyev, D. G. Cory, and C. Ramanathan, *Phys. Rev. Lett.*, 2008, **100**, 127601.

4.   M. Lelli, D. Gajan, A. Lesage, M. A. Caporini, V. Vitzthum, P. Miéville, F. Héroguel, F. Rascón, A. Roussey, C. Thieuleux, M. Boualleg, L. Veyre, G. Bodenhausen, C. Copéret, and L. Emsley, *J. Am. Chem. Soc.*, 2011, **133**, 2104–7.

5.   V. S. Bajaj, M. L. Mak-Jurkauskas, M. Belenky, J. Herzfeld, and R. G. Griffin, *J. Magn. Reson.*, 2010, **202**, 9–13.

6.   A. B. Barnes, G. De Paëpe, P. C. A. van der Wel, K. N. Hu, C. G. Joo, V. S. Bajaj, M. L. Mak-Jurkauskas, J. R. Sirigiri, J. Herzfeld, R. J. Temkin, and R. G. Griffin, *Appl. Magn. Reson.*, 2008, **34**, 237–263.

7.   E. J. Koers, M. P. López-Deber, M. Weingarth, D. Nand, D. T. Hickman, D. Mlaki Ndao, P. Reis, A. Granet, A. Pfeifer, A. Muhs, and M. Baldus, *Angew. Chemie Int. Ed.*, 2013, **52**, 10905–10908.

8.   T. Jacso, W. T. Franks, H. Rose, U. Fink, J. Broecker, S. Keller, H. Oschkinat, and B. Reif, *Angew. Chemie Int. Ed.*, 2012, **51**, 432–435.

9.   C.-Y. Cheng and S. Han, *Annu. Rev. Phys. Chem.*, 2013, **64**, 507–32.

10.   D. Shimon, Y. Hovav, A. Feintuch, D. Goldfarb, and S. Vega, *Phys. Chem. Chem. Phys.*, 2012, **14**, 5729–5743.

11.   K. R. Thurber, W.-M. Yau, and R. Tycko, *J. Magn. Reson.*, 2010, **204**, 303–313.

12.   W. Meyer, J. Heckmann, C. Hess, E. Radtke, G. Reicherz, L. Triebwasser, and L. Wang, *Nucl. Instruments Methods Phys. Res. Sect. A Accel. Spectrometers, Detect. Assoc. Equip.*, 2011, **631**, 1–5.

13.   H. Jóhannesson, S. Macholl, and J. H. Ardenkjaer-Larsen, *J. Magn. Reson.*, 2009, **197**, 167–175.

14.   C. Song, K.-N. Hu, C.-G. Joo, T. M. Swager, and R. G. Griffin, *J. Am. Chem. Soc.*, 2006, **128**, 11385–11390.

15.   K.-N. Hu, C. Song, H. Yu, T. M. Swager, and R. G. Griffin, *J. Chem. Phys.*, 2008, **128**, 52302–52317.

16.   A. Zagdoun, G. Casano, O. Ouari, M. Schwarzwälder, A. J. Rossini, F. Aussenac, M. Yulikov, G. Jeschke, C. Copéret, A. Lesage, P. Tordo, and L. Emsley, *J. Am. Chem. Soc.*, 2013, **135**, 12790–12797.

17.   T. Maly, G. T. Debelouchina, V. S. Bajaj, K.-N. Hu, C.-G. Joo, M. L. MakJurkauskas, J. R. Sirigiri, P. C. A. van der Wel, J. Herzfeld, R. J. Temkin, and R. G. Griffin, *J. Chem. Phys.*, 2008, **128**, 52211–52219.

18. T. A. Siaw, S. A. Walker, B. D. Armstrong, and S.-I. Han, *J. Magn. Reson.*, 2012, **221**, 5–10.

19. L. R. R. Becerra, G. J. J. Gerfen, B. F. F. Bellew, J. A. A. Bryant, D. A. A. Hall, S. J. J. Inati, R. T. T. Weber, S. Un, T. F. F. Prisner, A. E. E. McDermott, K. W. W. Fishbein, K. E. E. Kreischer, R. J. J. Temkin, D. J. J. Singel, and R. G. G. Griffin, *J. Magn. Reson. Ser. A*, 1995, **117**, 28–40.

20. S. Macholl, H. Johannesson, and J. H. Ardenkjaer-Larsen, *Phys. Chem. Chem. Phys.*, 2010, **12**, 5804–5817.

21. J. H. Ardenkjaer-Larsen, S. Macholl, and H. Jóhannesson, *Appl. Magn. Reson.*, 2008, **34**, 509–522.

22. L. Lumata, M. E. Merritt, C. R. Malloy, A. D. Sherry, and Z. Kovacs, *J. Phys. Chem. A*, 2012, **116**, 5129–38.

23. S. a Walker, D. T. Edwards, T. A. Siaw, B. D. Armstrong, and S. Han, *Phys. Chem. Chem. Phys.*, 2013, **15**, 15106–20.

24. Y. Matsuki, T. Maly, O. Ouari, H. Karoui, F. Le Moigne, E. Rizzato, S. Lyubenova, J. Herzfeld, T. Prisner, P. Tordo, and R. G. Griffin, *Angew. Chemie*, 2009, **121**, 5096–5100.

25. M. Rosay, V. Weis, K. E. Kreischer, R. J. Temkin, and R. G. Griffin, *J. Am. Chem. Soc.*, 2002, **124**, 3214–3215.

26. C. T. Farrar, D. A. Hall, G. J. Gerfen, M. Rosay, J. H. Ardenkjær-Larsen, and R. G. Griffin, *J. Magn. Reson.*, 2000, **144**, 134–141.

27. V. S. Bajaj, C. T. Farrar, M. K. Hornstein, I. Mastovsky, J. Vieregg, J. Bryant, B. Eléna, K. E. Kreischer, R. J. Temkin, and R. G. Griffin, *J. Magn. Reson.*, 2003, **160**, 85–90.

28. A. B. Barnes, M. L. Mak-Jurkauskas, Y. Matsuki, V. S. Bajaj, P. C. a van der Wel, R. Derocher, J. Bryant, J. R. Sirigiri, R. J. Temkin, J. Lugtenburg, J. Herzfeld, and R. G. Griffin, *J. Magn. Reson.*, 2009, **198**, 261–70.

29. V. S. Bajaj, M. L. Mak-Jurkauskas, M. Belenky, J. Herzfeld, and R. G. Griffin, *Proc. Natl. Acad. Sci.*, 2009, **106**, 9244–9249.

30. D. A. Hall, D. C. Maus, G. J. Gerfen, S. J. Inati, L. R. Becerra, F. W. Dahlquist, and R. G. Griffin, *Science (80-.).*, 1997, **276**, 930–932.

31. L. J. Berliner, S. S. Eaton, and G. R. Eaton, *Biological Magnetic Resonance: Volume 19: Distance Measurements in Biological Systems by EPR*, Springer, 2001.

32. Y. Zhou, B. E. Bowler, G. R. Eaton, and S. S. Eaton, *J. Magn. Reson.*, 1999, **139**, 165–174.

33. B. D. Armstrong, D. T. Edwards, R. J. Wylde, S. A. Walker, and S. Han, *Phys. Chem. Chem. Phys.*, 2010, **12**, 5920–5926.

34. S. Takahashi, L.-C. Brunel, D. T. Edwards, J. van Tol, G. Ramian, S. Han, and M. S. Sherwin, *Nature*, 2012, **489**, 409–413.

35. J. van Tol, L.-C. Brunel, and R. J. Wylde, *Rev. Sci. Instrum.*, 2005, **76**, 74101.

36. G. M. Smith, J. C. G. Lesurf, R. H. Mitchell, and P. C. Riedi, *Rev. Sci. Instrum.*, 1998, **69**, 3924–3937.

37. D. T. Edwards, S. Takahashi, M. S. Sherwin, and S. Han, *J. Magn. Reson.*, 2012, **223**, 198–206.

38. V. A. Atsarkin, *Sov. Phys. Uspekhi*, 1978, **21**, 725.

39. A. Abragam and M. Goldman, *Reports Prog. Phys.*, 1978, **41**, 395–467.

40. R. A. Wind, M. J. Duijvestijn, C. van der Lugt, A. Manenschijn, and J. Vriend, *Prog. Nucl. Magn. Reson. Spectrosc.*, 1985, **17**, 33–67.

41. Y. Hovav, A. Feintuch, and S. Vega, *Phys. Chem. Chem. Phys.*, 2013, **15**, 188–203.

42. Y. Hovav, O. Levinkron, A. Feintuch, and S. Vega, *Appl. Magn. Reson.*, 2012, **43**, 21–41.

43. Y. Hovav, A. Feintuch, and S. Vega, *J. Chem. Phys.*, 2011, **134**, 74509–74520.

44. Y. Hovav, A. Feintuch, and S. Vega, *J. Magn. Reson.*, 2010, **207**, 176–189.

45. Y. Hovav, A. Feintuch, and S. Vega, *J. Magn. Reson.*, 2012, **214**, 29–41.

46. M. Borghini, *Phys. Rev. Lett.*, 1968, **20**, 419.

47. D. Banerjee, D. Shimon, A. Feintuch, S. Vega, and D. Goldfarb, *J. Magn. Reson.*, 2013, **230**, 212–219.

48. S. Chandrasekhar, *Rev. Mod. Phys.*, 1943, **15**.

49. S. Takahashi, R. Hanson, J. van Tol, M. Sherwin, and D. Awschalom, *Phys. Rev. Lett.*, 2008, **101**, 047601.

50. H. Sato, V. Kathirvelu, G. Spagnol, S. Rajca, A. Rajca, S. S. Eaton, and G. R. Eaton, *J. Phys. Chem. B*, 2008, **112**, 2818–2828.

51.   K. R. Thurber and R. Tycko, *J. Chem. Phys.*, 2014, **140**, 184201.

52.   K. R. Thurber and R. Tycko, *J. Chem. Phys.*, 2012, **137**, 84508–84514.

53.   S. Stoll, B. Epel, S. Vega, and D. Goldfarb, *J. Chem. Phys.*, 2007, **127**, 164511.